V. Muscarello, G. Quaranta
Exploration of the Effects of Rotor Blade Twist on Whirl-Flutter Stability Boundaries
Journal of Aircraft, published online 18/09/2023
doi:10.2514/1.C037479

Exploration of the Effects of Rotor Blade Twist on Whirl-Flutter Stability Boundaries

Vincenzo Muscarello*
Royal Melbourne Institute of Technology, Melbourne, VIC, 3082, Australia

Giuseppe Quaranta†
Polytechnic University of Milan, 20156 Milan, Italy

This paper investigates the influence of tiltrotor blade twist on whirl-flutter stability boundaries. Preliminary evaluations indicate that the whirl-flutter speed can be increased if the blade twist slope is reduced. This positive effect results from the shift in the overall thrust toward the blade tip, increasing the flapwise bending moment at the blade root and the trim coning angle. This, in turn, generates a positive pitch-lag coupling, increasing the whirl-flutter speed. However, the shift of high sectional thrust forces toward the blade tip sections returns a higher induced drag, showing the tendency to increase the power required.

The paper shows that by using blade twist laws based on piecewise linear functions and adding the wing airfoil thickness as a second design parameter, it is possible to identify aircraft configurations that improve the whirl-flutter stability boundaries without penalizing the power required in airplane and helicopter mode flight. This is possible because the blade twist and the wing airfoil thickness have an impact on both power required and whirl-flutter speed, so a simple optimization algorithm can identify good trade-offs.

A detailed tiltrotor model representative of the Bell XV-15 is used to display the effectiveness of the proposed approach. The examples show that increases up to 21% on the whirl-flutter speed are achievable without penalties in the aircraft power required and with the additional benefit of a benign impact on rotor pitch link loads.

Nomenclature

A_s = Wing stringer area, in^2

C_D^{WP} = Wing-Pylon drag coefficient

C_L^{WP} = Wing-Pylon lift coefficient

EJ_b = Wing beam bending stiffness, $\text{lb}\cdot\text{in}^2$

Presented as Paper 2023-1510 at the 2023 AIAA Science and Technology Forum, National Harbor, MD, January 23–27, 2023.
*Senior Lecturer, Aerospace Engineering and Aviation, vincenzo.muscarello@rmit.edu.au, AIAA Member, Corresponding author.
†Full Professor, Department of Aerospace Science and Technology, giuseppe.quaranta@polimi.it, AIAA Member.

EJ_c = Wing chord bending stiffness, lb·in^2

FM = Figure of merit

GJ = Wing torsional stiffness, lb·in^2

K_{p_ζ} = Pitch-lag coupling, positive for lag back, pitch down

M = Mach number

P = Rotor power, hp

P_{ms} = Rotor power evaluated at the maximum safe flight speed, hp

r_i = Radial station where the blade twist slope change takes place, r/R

T = Rotor thrust, lb

t_b = Wing skin thickness, in

t_h = Wing spar thickness, in

t/c = Thickness to chord ratio

V_{ms} = Maximum safe flight speed, knots

V_{wf} = Whirl-flutter speed, knots

β_0 = Collective flap angle, deg

β_{1C}, β_{1S} = Cyclic cosine and sine flap angles, deg

β_{GC}, β_{GS} = Longitudinal and lateral gimbal angles, deg

ζ_0 = Collective lead-lag angle, deg

ζ_{1C}, ζ_{1S} = Cyclic cosine and sine lead-lag angles, deg

ϑ_0 = Collective pitch angle, deg

$\vartheta_{1C}, \vartheta_{1S}$ = Cyclic cosine and sine pitch angles, deg

ϑ_{tw} = Blade twist, deg

ϑ'_{tw_i} = Blade twist slope, deg/(r/R)

ξ = Damping ratio, %

ω = Frequency, Hz

I. Introduction

Tiltrotors are aircraft designed to overcome the speed and range limits affecting conventional helicopters by using the rotors only for the generation of lift at low speed (helicopter mode) and transforming them into thrust generators at high speed, where the lift is provided by the aircraft wing (aircraft mode). However, at high speeds in airplane mode, whirl flutter is still a major performance limitation for tiltrotors.

Whirl flutter is an aeroelastic instability that affects flexibly mounted aircraft engine-propeller combinations. It was

discovered in 1938 as a precession-type instability in turboprop aircraft configurations [1]. The correct analysis requires taking into account the influence of rotating masses producing centrifugal, Coriolis, and gyroscopic forces/moments in addition to the aerodynamic loads. The fundamental problem is a not symmetrical distribution of lift force on the transversely vibrating propeller that may cause unstable vibrations or even a failure of the engine or the supporting wing structure. The basic phenomenon is described in detail by Wilmer H. Reed III in Ref. [2].

Nixon in Ref. [3] showed how a wide enough separation between the torsional and the beam bending* frequencies is essential to ensure aeroelastic stability. Indeed, the analysis performed in Ref. [3] demonstrated that if the wing beam bending stiffness is increased (e.g. $EI_b^{\text{new}} = 1.5 \times EI_b$), the flutter speed decreases unless the torsional stiffness is also increased (that is, $GJ^{\text{new}} \geq 1.3 \times GJ$).

With the current technology, very stiff (and thick) wings of limited aspect ratio are used to meet the stability requirements, severely limiting cruise efficiency and maximum speed [4]. Many current designs that fly like the V-22, or have flown like the XV-15, have a 23% thick wing to ensure a whirl-flutter speed well beyond the dive speed. Increased power, thrust, and rotor efficiency are of no avail unless the whirl-flutter stability can be improved. Consequently, many research efforts have been dedicated to improving the whirl-flutter speed boundaries of tiltrotors. Tailoring of wing stiffness using composite material has been shown to be quite effective in extending the whirl-flutter boundaries [5–7]. In [5], the usage of composite materials influencing the pitch/bending coupling allows using an 18% thin wing that exceeds the whirl-flutter boundaries of the baseline wing by 12 knots. A more extensive application of aeroelastic tailoring for stability augmentation, not only on the wing but also on the rotor blades, was considered in [7] showing very promising results. Different approaches exploited the usage of active stability augmentation systems to obtain an increment of the whirl-flutter-free envelope [8–10]. In other cases, the modification of the aircraft architecture was sought, including the inclusion of wing extensions or winglets [11], that combined with a modification of structural characteristics of the wing has been shown to achieve a remarkable 22% improvement in the whirl-flutter speed.

A different approach was proposed by Acree et al. [12] where the improvement in whirl-flutter speed was obtained by adjusting the chordwise positions of the rotor blade aerodynamic center (AC), the airfoil quarter chord (QC), and the center of mass (CM). The modification of the position of the AC of an airfoil is possible by changing the geometry but is typically limited to very small adjustments while moving CM requires the addition of masses and the moving of the airfoil QC with respect to the blade feathering axis can be obtained through sweep angles, typically close to the blade tip. However, the last two types of modifications may bring in other drawbacks, such as heavier blades or higher pitch-link loads, so they have to be exerted with care. The baseline aircraft model used in [12] was the XV-15 tiltrotor with a 15% thickness modified wing, which brought the whirl-flutter speed at 275 knots. Large improvements of the stability boundaries were achieved in [12] with an increase of the whirl-flutter speed up to 100 knots, equal to a 36% improvement, although several drawbacks, due to the excessive increase in pitch link loads, could have caused a

*In tiltrotors, the term “beam bending” commonly refers to “out-of-plane bending” while “chord bending” refers to “in-plane bending”.

potential limit to the advantages. However, the analysis contained in [12] pointed out that a change in aerodynamic load distribution on the blades can affect significantly the whirl-flutter stability. Gul and Datta [13] showed that such a change can be beneficial also for hingeless hub tiltrotors and not only for classical gimballed hub ones, as is the case presented here.

Further investigations in this direction showed that among the aerodynamic parameters of the rotor, the blade twist could be quite effective in moving the whirl-flutter speed forward, with improvements up to 20% [14]. However, those improvements have the downside of increasing the power required, nullifying the potential improvement on the whirl-flutter-free envelope. To better investigate the potential of the rotor twist as a means to improve the overall performance of a tiltrotor, it is proposed here to include more design parameters that affect the whirl-flutter speed and the power required and tackle the problem through a simple multidisciplinary optimization, as those proposed in [15–18]. However, differently from [15, 18] where the objective of the optimizations was to try to improve the aerodynamic efficiency of the rotor or the entire aircraft – including both hover and high-speed flight conditions – while reducing weight under aeroelastic stability constraints, here the objective is inverted, i.e. trying to improve the stability boundaries of the aircraft while keeping the power required below the maximum power of the baseline model. The objective of this change of point of view is twofold: a) first, it is possible to focus on the effect of blade twist on aeroelastic stability since the effect on power required is well known, because a basic understanding of the physical mechanism associated with this improvement may be of better help than the research of an optimal configuration for a specific aircraft; b) second, to focus more on maximizing the whir-flutter speed, leaving the choice between the two options of keeping the same flight envelope with a lower power required, or expanding the flight envelope with the same power, to the analysis of specific operative missions of the aircraft under investigation.

The idea of looking at blade twist change as a means to improve tiltrotor performance is not new. In Ref. [7] a mechanism to change the blade twist to adapt it when switching from helicopter mode to airplane mode was presented. However, the problem was analyzed from the point of view of better rotor efficiency, i.e. power required, and tackled with composite-made extension-twist-coupled blades that presented many aeroelastic drawbacks. Indeed, the dominant effect was associated with the pitch-lag coupling in the rotor system, created by the tip-weight in combination with precone, and a reduction in the rotor thrust between hover and cruise. This effect resulted in a large negative spring relating the torsion moment about the pitch axis to blade lag deformation, reducing the whirl-flutter speed by at least 50%. No direct analysis of the effect of twist on aeroelastic stability was conducted. A similar objective was sought in [19], where shape memory alloy hybrid composite materials were used. However, both papers showed that potentially it is possible to design and manufacture a morphing system able to adapt the twist of the blades to the flight condition.

As a baseline for this study a detailed aeroelastic tiltrotor model is used, representative of the Bell XV-15 with Advanced Technology Blades (ATBs). It has been assembled in CAMRAD/JA using data published in Ref. [20]. Multidisciplinary optimization is implemented with the objective function to maximize the whirl-flutter speed, under

power constraints. The optimization considers the wing airfoil thickness along with different laws for rotor blade twist based on piecewise linear functions as the design variables, trying to exploit the idea that even if the twist brings higher aeroelastic stability boundaries at the expense of more power required, this could be traded by the optimizer to reduce the wing airfoil thickness that has the opposite effect but may affect whirl-flutter stability. It has been decided to not consider hover performance in the optimization at this stage. However, a post-optimality assessment in helicopter mode flight is presented as well, showing that the impact is benign.

The paper proceeds as follows: section II is dedicated to the description of the dynamic model setup. The many substructures that are part of the CAMRAD/JA aeroelastic model (airframe structural dynamics, airframe aerodynamics, aeroelastic rotors, engine-drive train system, and the governor controller) are outlined. The modifications of the wing structural and aerodynamic characteristics concerning different thickness-to-chord ratios are presented as well. Section III summarizes the results obtained using the blade twist as the only design variable , explaining the physical mechanism that is at the root of the whirl-flutter stability increase obtained. Section IV presents a detailed overall aircraft optimization with more design variables, including the wing airfoil thickness together with different blade twist configurations. The last section brings the paper to closure by drawing conclusions about the work performed.

II. Model Setup

A detailed tiltrotor model, representative of the Bell XV-15 research aircraft with advanced technology blades (ATBs) [21], has been built in CAMRAD/JA [22] using data published by Acree in Ref. [20]. The dynamic model set-up includes 1) the airframe structural model, 2) the airframe stability and control derivatives, 3) aeroelastic rotors, and 4) a lumped parameter engine drive-train governor system. While in Ref. [23] it was shown that the addition of pilots' biodynamics may give a further contribution to whirl-flutter speed, it was decided to not consider this effect in this specific case to allow comparisons with results published by other authors. The XV-15 general characteristics are summarized in Table 1.

This section presents the dynamic model setup and validation together with the extension done to model the wing with a variable thickness, necessary to run the following optimizations.

A. Tiltrotor Aeroelastic Model

The layout of the Bell XV-15 is similar to a turboprop aircraft. Large proprotors, coupled with turboshaft engines, are mounted on the wingtip nacelles. The rotor axis rotates from the vertical direction, used for hover and helicopter mode flight (HEMODE), to the horizontal direction, used for airplane mode flight (APMODE). According to Ref. [12], the airframe structure can be modeled using a finite element (FE) stick model consisting of an elastic wing, a rigid fuselage, rigid wing-mounted nacelles, plus the inertial effect of rotors represented through two lumped masses. The resulting FE model is depicted in Fig. 1.

Table 1 XV-15 general characteristics.

Characteristic	Symbol	XV-15 (ATBs)	Units
Gross takeoff weight	W_{TO}	13,000	lb
Maximum engine(s) power	P_{max}	2×1,550	hp
Maximum flight speed	V_{max}	280	knots
Wing span	b	32.17	ft
Wing area	S	181.0	ft^2
Rotor radius	R	12.50	ft
Rotor solidity	σ	0.103	n.d.
Rotor Lock number	γ	3.768	n.d.
Rotor rotating speed	Ω	601[a]	rpm

[a] Reduced to 480.8 rpm in airplane mode.

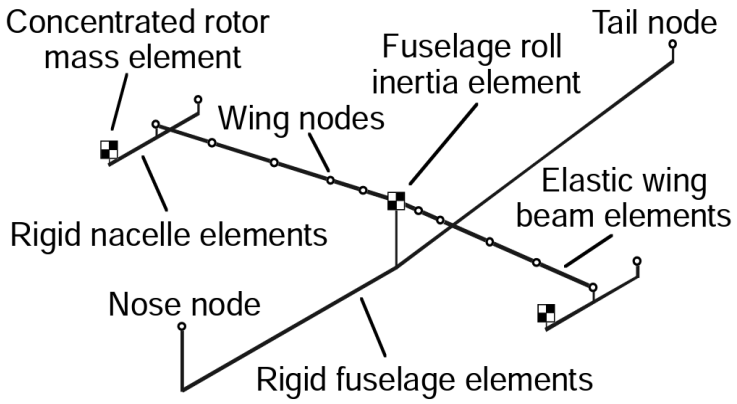

Fig. 1 Bell XV-15 airframe finite element stick model [12].

The airframe model aims at capturing the fundamental six normal modes of the wing that contribute to the whirl-flutter mechanism, i.e. symmetric/antisymmetric wing bending (SWB/AWB), symmetric/antisymmetric wing chord (SWC/AWC), and symmetric/antisymmetric wing torsion (SWT/AWT). The natural frequencies and mode shapes are obtained using NASTRAN. Table 2 lists the frequencies in HEMODE and APMODE for the 15% thin-wing proposed by Acree et al. in Ref. [12]. The airframe modes considered for whirl-flutter analyses are the first of each type.

The airframe aerodynamics are modeled through the aerodynamic lookup tables of the wing-body, horizontal tail, and vertical tails provided by Ferguson in Ref. [24]. Lift, drag, and moment coefficients are reported as a function of the angle of attack, Mach number, and nacelle angle. With these data, it is possible to generate the complete database of airframe stability and control derivatives in CAMRAD/JA, which is essential to find the correct trim condition for the aircraft at different flight speeds. The choice to use a quasi-steady model for the airframe aerodynamics stemmed mainly from the necessity to obtain results comparable with those presented in Ref. [12]. Full unsteady airframe aerodynamics could be adopted for whirl-flutter analysis, as shown in [25]. However, the effect of wing unsteady aerodynamic loads

Table 2 XV-15 airframe natural frequencies in HEMODE and APMODE, with 15% thin-wing.

	HEMODE	APMODE
Mode	Frequency, Hz	Frequency, Hz
SWB	2.22	2.34
AWB	4.49	4.48
SWT	5.17	6.09
AWT	5.37	5.61
SWC	6.53	5.07
AWC	7.56	7.03

has been considered negligible at this stage.

The XV-15 ATBs rotors used in the study are characterized by composite blades, with a +1.5 deg. precone angle and a negative pitch-gimbal kinematic coupling (δ_3 = -15 deg). Rotor blade aerodynamic forces are calculated using lifting line theory and steady, two-dimensional airfoil characteristics, with corrections for unsteady and three-dimensional flow effects (Ref. [22]). C81 tables are provided by Acree in Ref. [20], in which lift, drag, and pitching moment coefficients related to the XV-15 ATBs are tabulated versus the angle of attack, covering the entire ±180° range, and several Mach numbers ranging from 0 to 1. The momentum theory induced velocity model is also included; empirical corrections to account for nonideal induced power losses and a linear variation of the induced velocity over the rotor disk due to nonaxial flow are defined in Ref. [20] as well as a tip loss factor for three-dimensional flow effects. Quasi-steady lift and moment coefficients are also implemented in CAMRAD/JA based on unsteady thin airfoil theory (see Ref. [22], chapter 2). Collective and cyclic modes have been considered for the three-bladed, gimballed, stiff-in-plane XV-15 rotors, respectively: two bending modes, one torsion mode, and two gimbal modes (longitudinal and lateral). According to Ref. [26], for proprotor stability analysis, only the fundamental modes below 1/rev are important. The two bending and the gimbal modes are selected to model the rotor cyclic flapping, lead–lag, and rotor coning modes that lie in the frequency range of interest. The first torsion mode is related to control chain compliance. This mode also provides the kinematic pitch-gimbal and pitch-bending couplings designed to reduce flapping and to keep the rotor flapping mode below 1/rev, reducing flap/lag instability in tiltrotors (Ref. [27]). Please, note that the gimbal universal joint in CAMRAD/JA has been modeled as an ideal homokinetic joint, neglecting the 2/rev components caused by rotor flapping (Ref. [28]). Additionally, the three-state Pitt–Peters dynamic inflow model (Ref. [29]) and the rotor speed degree of freedom have been taken into account. Thus, each rotor model contains 15 degrees of freedom. The two rotors operate at 601.0 rpm (100%) in helicopter and conversion modes. Once fully converted to airplane mode, the rotor speed is decreased to 480.8 rpm (80%). Table 3 shows the fundamental rotor frequencies in a vacuum, for the two rotor speeds. Except for the regressive gimbal and lead-lag modes, all the rotor modes are placed above 10 Hz, far away from the fundamental elastic wing modes.

Table 3 XV-15 rotor frequencies in vacuum.

	HEMODE			APMODE		
	100% rpm, ϑ_0 = 12 deg			80% rpm, ϑ_0 = 40 deg		
Mode	Coll. Hz	Reg. Hz	Prog. Hz	Coll. Hz	Reg. Hz	Prog. Hz
Gimbal	–	0.19	20.22	–	0.24	16.27
1^{st} Bending (Lag)	12.68	3.18	23.22	10.19	2.42	18.45
2^{nd} Bending (Flap)	16.03	17.90	37.93	15.94	22.85	38.88
1^{st} Torsion	30.39	20.85	40.88	28.87	20.44	36.47

The dynamics of the engine-drive train system are modeled with simplified one-dimensional models consisting of a set of torsional springs and equivalent lumped inertias as shown in Fig. 2, using data provided by Acree [20]. The XV-15

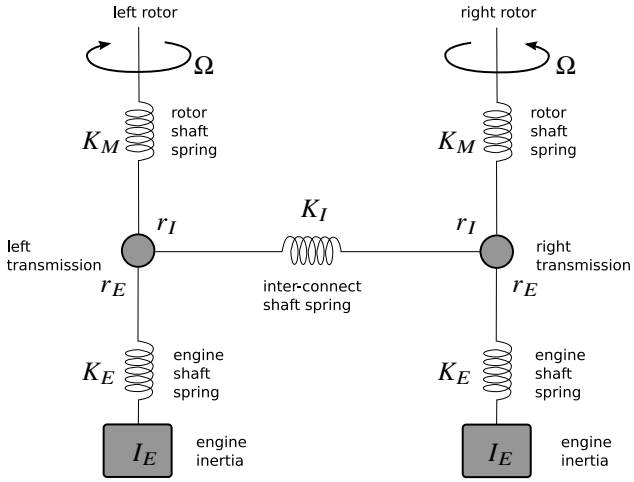

Fig. 2 Symmetric engine-drive train model.

reduced parameters I_E, K_E, K_M, K_I and the gear ratios, i.e. r_I and r_E, are derived from Ref. [20]. The two gearboxes are joined by an interconnecting shaft. This system precludes the complete loss of power to either rotor due to a single engine failure, permits power transfer for transient conditions, and provides rotational speed synchronization (Ref. [30]).

The XV-15 engine-drive system's natural frequencies are listed in Table 4. The long interconnect drive shaft causes

Table 4 XV-15 engine-drive system natural frequencies.

Mode	Frequency, Hz
1^{st} antisymmetric	4.50
1^{st} symmetric	13.98
2^{nd} antisymmetric	16.62

the first anti-symmetric drive system mode to be in the frequency range of the fundamental wing modes, and thus potentially important for whirl-flutter stability. Details on the modeling of this subsystem can be found in Refs. [31, 32],

including the “Beta” governor control laws.

B. Wing Model

To consider the wing airfoil thickness as an optimization variable, it is necessary to allow the modification of the wing structural and aerodynamic characteristics in the aeroelastic model, as discussed in the following subsections.

1. Structural Model

Starting from the design proposed in Ref. [12], it has been decided to modify only the thickness of the wing section, without changing any other parameter. The design for a 15% thin-wing proposed by Acree et al. [12] is different from the one of the original aircraft and uses composite graphite-epoxy structural components. The original design was based on a NACA 64A223 airfoil, and [12] considered a single torque box model for the wing structure, scaling down the coordinates of the airfoil to reduce the maximum thickness from 23% to 15%. A simple semi-monocoque idealization, with constant shear flow panels and linearly varying axial force stringers (see Ref. [33], Chapter 20) can be used to assess the structural stiffness. The single torque box structure used here is represented in Fig. 3 and is composed of 8 panels and 8 stringers where the area of panels and stringers is lumped. Choosing as material properties those presented

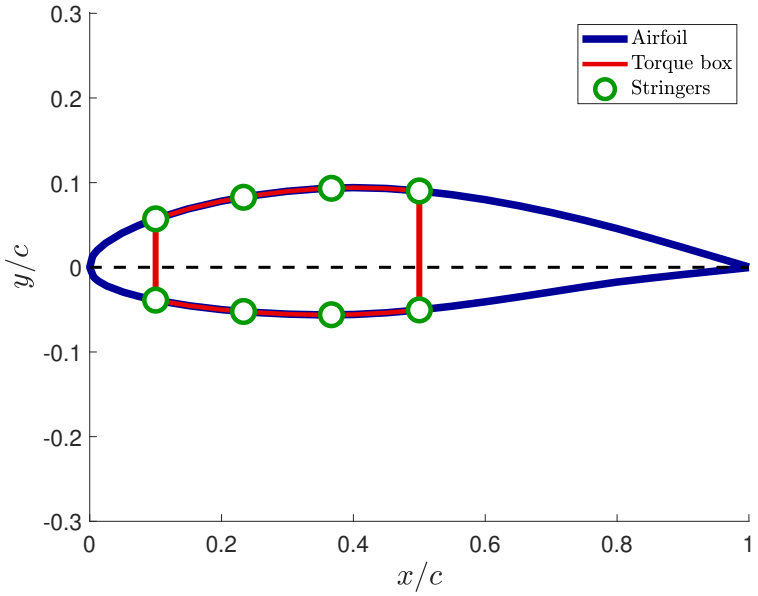

Fig. 3 Torque box used to estimate the semi-monocoque characteristics of the structural section with 15% thickness airfoil.

in Table 5, and as target stiffnesses those used in the 15% thin-wing model of [12], reported in Table 6, it has been possible to solve an inverse design problem to guess the section geometric characteristics, i.e. skin and spar thicknesses, and stringer areas. Details on the process may be found in Ref. [34]. Keeping the material properties constant while changing the wing airfoil thickness it is possible to compute how the stiffnesses are modified. The torsional stiffness

Table 5 Reference material properties used for graphite-epoxy composite structure, Ref. [12].

Property	Symbol	Unit	Value
Elastic modulus, torque box	E_t	lb/in^2	9.00×10^{6}
Elastic modulus, stringers	E_s	lb/in^2	18.00×10^{6}
Shear modulus, torque box	G	lb/in^2	3.75×10^{6}
Density	ρ	lb/in^3	6.00×10^{-2}
Limit strain	ϵ_{max}	in/in	0.47×10^{-2}

Table 6 Target sectional stiffnesses (Ref. [12]) and section geometric characteristics for the 15% thin-wing tiltrotor structure.

Property	Symbol	Units	Value
Beam bending stiffness	EJ_b	lb·in^2	1.98×10^{9}
Chord bending stiffness	EJ_c	lb·in^2	7.59×10^{9}
Torsional stiffness	GJ	lb·in^2	1.33×10^{9}
Stringer area	A_s	in^2	3.72×10^{-1}
Skin thickness	t_b	in	1.36×10^{-1}
Spar thickness	t_h	in	7.68×10^{-2}

(see Fig. 4(a)) almost doubles when moving from a 15% thin wing to a 24% thick wing, showing a very similar behavior as the one presented in [12]. This is expected since the torsional stiffness strongly depends on the square of the cell area [33]. The beam bending stiffness is instead increased by only 23%, ranging from a 15% thin- to a 24% thick-wing, leading to limited modification of the beamwise stiffness and associated beam bending mode frequencies (see Fig. 4(b)). For the chord bending stiffness, the variations are so small that it has been chosen to keep it constant.

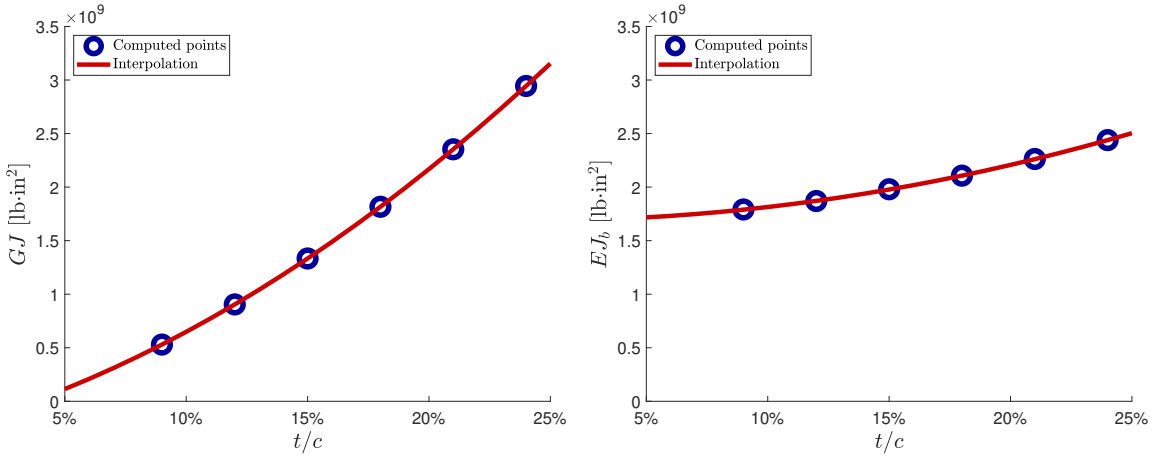

(a) Torsional stiffness. (b) Beam bending stiffness.

Fig. 4 Changes of bending and torsional stiffnesses with reference to wing airfoil thickness.

To this extent, it is possible to compute the stiffness for different values of wing airfoil thickness and then define an interpolation law to generate the updated NASTRAN structural models of the tiltrotor airframe structure for any wing

airfoil thickness ranging between 15% and 24%. The following interpolation laws have been identified for usage in the optimization process:

$$GJ = \left(30.050 \cdot (t/c)^2 + 6.182 \cdot (t/c) - 0.270\right) \times 10^9, \tag{1a}$$

$$EJ_b = \left(13.297 \cdot (t/c)^2 - 0.059 \cdot (t/c) + 1.687\right) \times 10^9. \tag{1b}$$

It must be remarked that the wing structure mass is not modified. Indeed, an increase in wing airfoil thickness leads to larger beam-bending and torsional stiffness without penalties in terms of wing weight since the skin and spar thicknesses, together with the stringers areas, remain constant. The modification of the wing airfoil thickness, however, affects offsets and cross-sectional moments of inertia. These contributions have not been included in the XV-15 airframe FE stick model. Indeed, cross-sectional rotatory inertia provides a secondary order effect with negligible impact on the first frequencies and mode shapes of the XV-15 airframe, required for whirl-flutter stability analyses. These assumptions hold for all structures characterized by high slenderness ratios [35].

The airframe natural frequencies in APMODE, with reference to the wing airfoil thickness, are depicted in Fig. 5. As expected, the increment in the wing airfoil thickness increases the symmetric and antisymmetric wing torsion natural

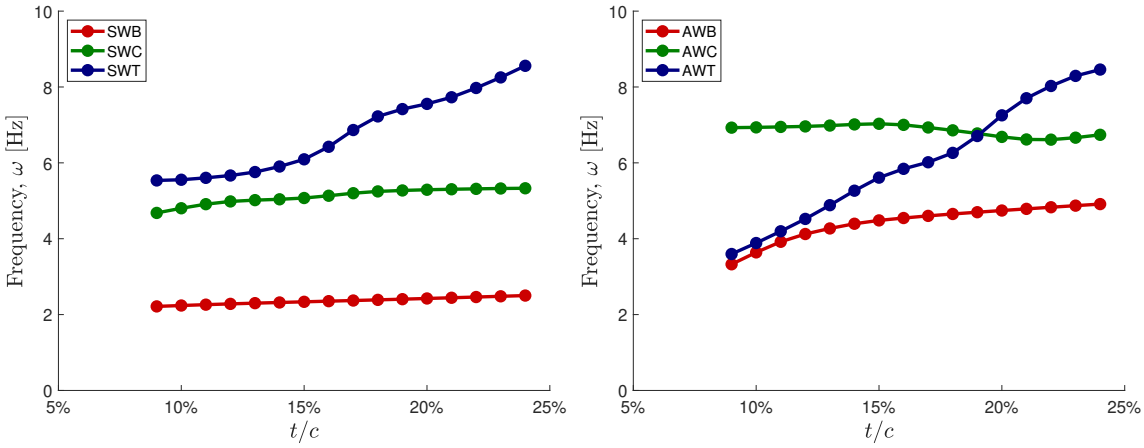

(a) Symmetric frequencies.

(b) Antisymmetric frequencies.

Fig. 5 Evolution of the symmetric (left) and antisymmetric (right) frequencies with reference to the wing airfoil thickness.

frequencies while the impact on the beamwise and chordwise bending modes is less remarked. The large torsional stiffness helps to reduce the pylon pitch motion, thereby increasing whirl-flutter stability. However, a thick wing design increases aerodynamic drag, limiting the cruise efficiency and maximum speed of the aircraft.

2. Aerodynamic Model

When the wing airfoil thickness changes, the aerodynamic characteristics are modified as well, with a significant impact on the aircraft performance and trim conditions. In particular, the rotor thrust and, consequently, the power required are both affected due to the change of aerodynamic drag at high speed.

A simple model of the wing was built using the software XFRL5[†] based on Prandtl lifting line theory (see [36], Chapter 8), joined with the airfoil aerodynamics characteristics obtained using XFOIL [37]. The Prandtl-Glauert correction was used to keep into account compressibility effects [38]. The results in terms of lift coefficient in the linear region are in very good agreement when compared to the experimental data provided by Ferguson in Ref. [24], at all Mach numbers. Instead, the resulting wing polars have been calibrated including an additional correction term to improve the fitting of the experimental wind tunnel results. This correction was necessary to consider the drag due to the nacelles. As a consequence, an additional contribution on the drag coefficient, constant for all angles of attack and set to $\Delta C_D^{WP} = 0.0105$, was added. This contribution remains constant up to $M = 0.5$ and suddenly increases at $M = 0.6$, reaching a value almost three times higher, $\Delta C_D^{WP} = 0.0290$.

Figure 6 shows the comparisons of the lift and drag coefficients between the XFRL5 model for a 23% thick-wing and the wind tunnel data [24]. These results show that the matching for the drag coefficient is fairly good in the range of low angles of attack, that is the range of interest in this work where the focus is on trimming the aircraft at high-speed flight conditions.

Figure 7 shows the lift and drag coefficients computed at Mach 0.2 for different values of wing airfoil thickness, to be used for the optimization process. The wing-pylon aerodynamic coefficients have been obtained for several Mach numbers in the range of $M = 0.1 - 0.6$. For any value of thickness or Mach number in the considered range, the coefficients to be used can be obtained using a simple two-dimensional interpolation routine.

C. Trim Criteria

In usual whirl-flutter flight-test operations, the aircraft is trimmed in level flight conditions up to the power-limited – or in some cases torque-limited – airspeed. Then, to increase the speed, it is allowed to follow a descent trajectory necessary to achieve the desired airspeed. However, in some cases, the zero-power (windmill) state is the limiting condition for whirl-flutter stability. So this condition too must be included in the analysis.

In this work, three different trim conditions are employed in the analyses:

- Level flight with unlimited power;
- Level flight with limited power, that allows the aircraft to descend whenever exceeded the maximum power;
- Zero–power flight conditions (windmill state).

The first is unrealistic while the last must be always considered as a special case of constant power, representing a

[†]`http://www.xflr5.tech` visited on November 2022.

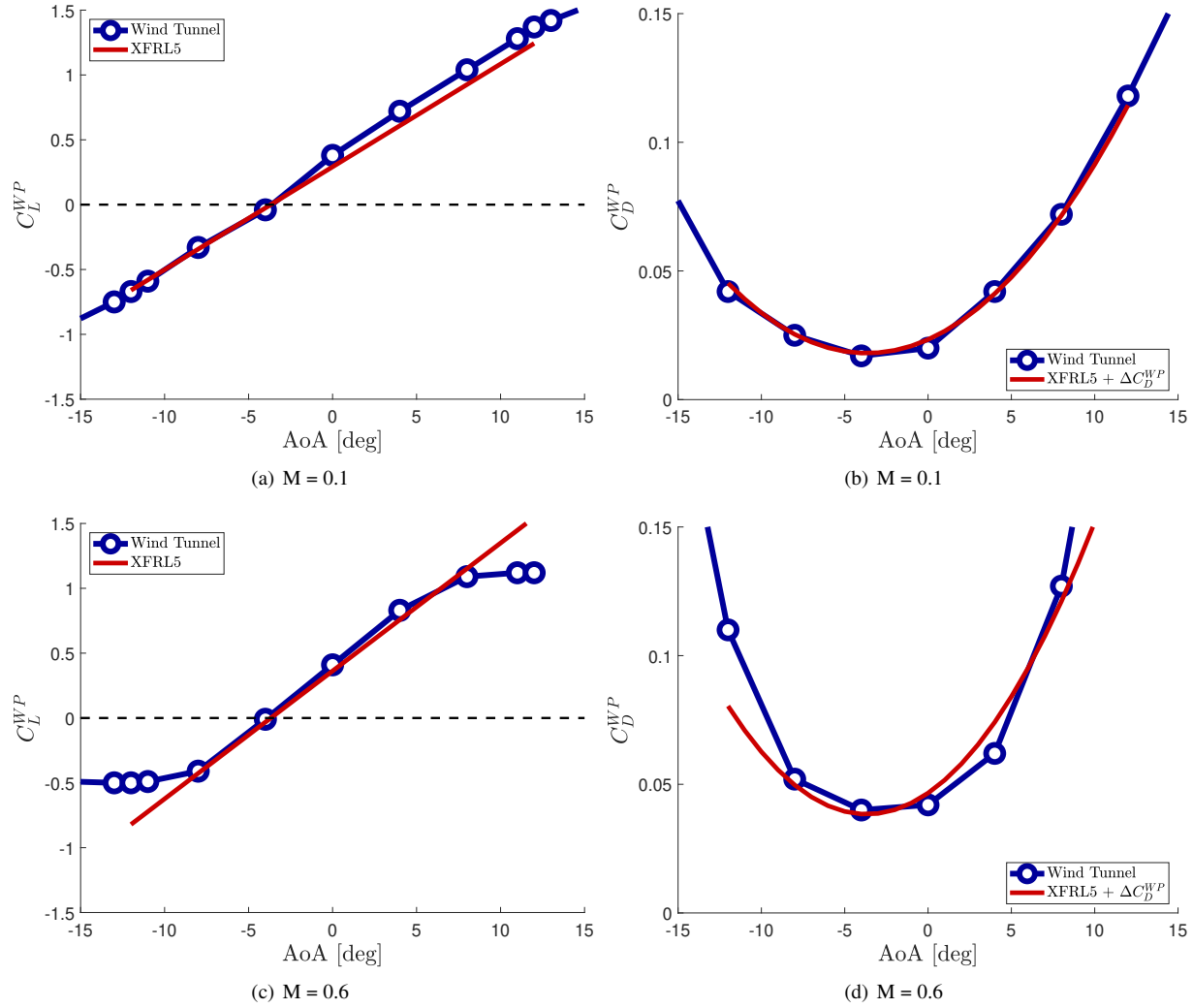

Fig. 6 Wing-pylon aerodynamic coefficients w.r.t. Angle of Attack (AoA): experimental [24] vs numerical data - 23% thick-wing.

possible emergency flight condition (engine out). For the XV-15 model with ATB, the whirl-mode stability boundaries are achieved with the zero-power condition [14], although the difference in whirl-flutter speed compared to other trim conditions is marginal. It can be speculated that, if the optimal wing airfoil thickness and blade twist configuration improve the whirl-flutter boundaries in level flight conditions with limited/unlimited power, then they also increase the whirl-flutter speed at zero–power conditions. For this reason, the optimizations are run only for powered cases.

Each rotor is trimmed to 480.8 rpm (80% of hover design rpm) at Sea Level Standard (SLS) ISA[‡] + 0° C flight conditions. The flight speed range considered is from 140 to 400 knots, with trim and stability calculated in 20-knot increments. Stability analyses consider all the rotor degrees of freedom, the airframe rigid body modes, the first 6 wing elastic modes, the engine-drive train dynamics, and the governor controller. Structural, modal damping of 1.5% has

[‡]International Standard Atmosphere

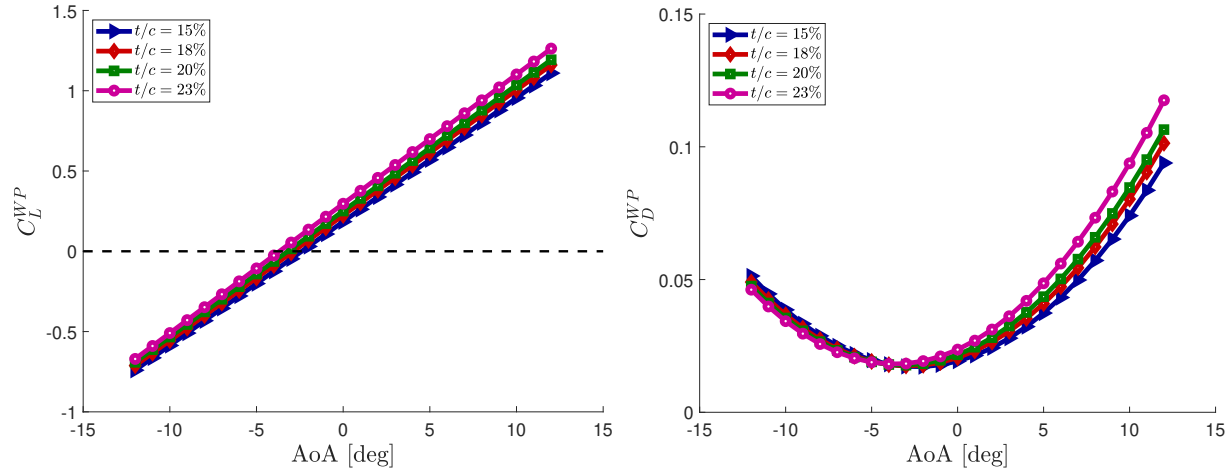

(a) Wing-Pylon lift coefficient.

(b) Wing-Pylon drag coefficient.

Fig. 7 Computed wing-pylon lift and drag coefficients for several wing airfoil thicknesses at $M = 0.2$.

been considered for each wing elastic mode.

III. Preliminary Rotor Parametric Analysis

To understand the physical mechanism at the basis of the stabilizing effect associated with blade twist, a simple modification on the XV-15 blade twist law is presented in the following. The baseline twist can be approximated by a constant slope of ϑ'_{tw_0} = -41.086 deg/(r/R). Two modified linear twist distributions are proposed by changing the slope of the linear twist by ±20%. All modified twist configurations have been defined to obtain the twist at 75% of the blade span equal to zero when considering null collective pitch. The modified configurations are named respectively "Twist+" and "Twist−". The three twist distributions are compared in Fig. 8. For the level flight condition with unlimited power,

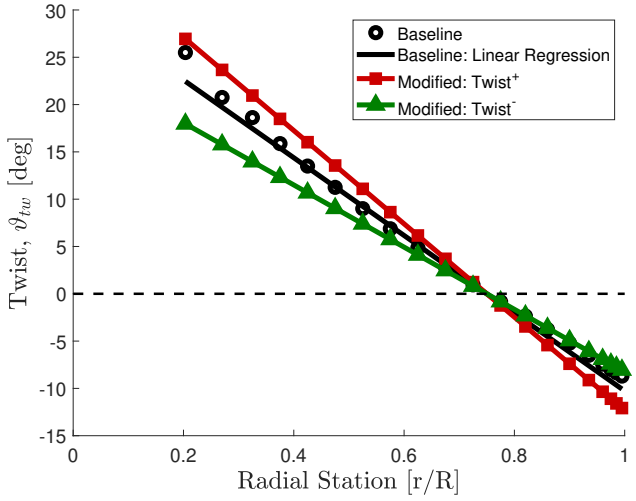

Fig. 8 Baseline and modified blade twist distributions.

with 15% thin-wing, the trim analysis returns almost the same values of pitch attitude and rotor thrust with reference to the flight speed for all three configurations, although slightly different collective pitch and elevator angles are obtained (see Ref. [14] for more details). Given the non-optimal choice of the twist, the modified configurations typically require

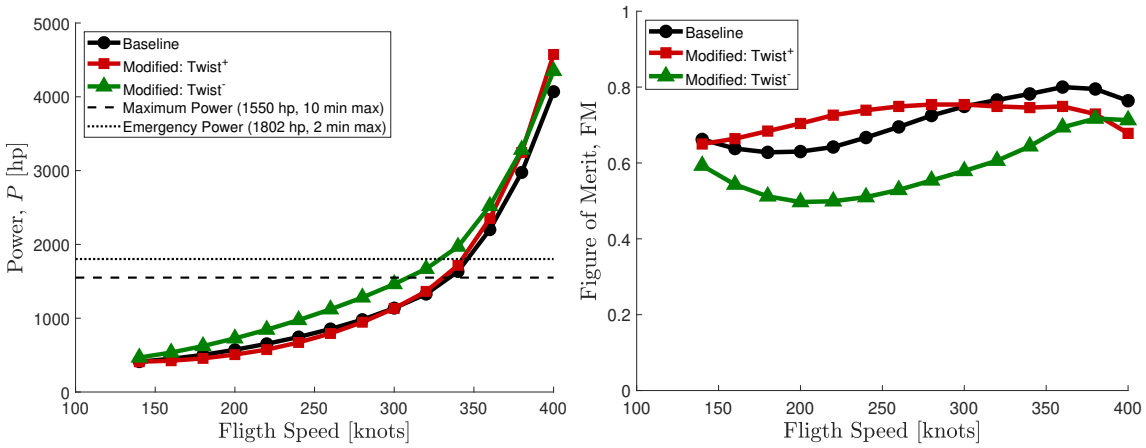

(a) Power.

(b) Figure of Merit.

Fig. 9 Trim results – level flight with unlimited power, 15% thin-wing.

more power, especially for the "Twist−" law (see Fig. 9(a)), reducing the proprotor efficiency (Fig. 9(b)). The latter is measured through the so-called Figure of Merit (FM), defined as the ratio of the minimum possible power to flight (i.e. the induced power) to the total power, which also includes the profile power (see Ref. [39], Chapter 3).

The evolution of the aeroelastic eigenvalues originating from the six wing elastic modes is discussed in the following. Each aeroelastic eigenvalue is labeled according to the structural mode that mainly participates in its corresponding aeroelastic eigenmode.

As predicted by Acree et al. [12], the unstable roots are the symmetric wing chord (309 knots) and antisymmetric wing bending modes (306 knots), shown in Fig. 10, although the corresponding whirl-flutter speeds for the XV-15 with ATBs are slightly higher when compared with those obtained in Ref. [12], referred to the XV-15 with metallic blades. The most critical whirl-flutter onset is caused by the AWB mode. At 380 knots, the blade tip airfoils reach the transonic regime. The blade section lift-curve slope is decreasing at that point, improving stability. This effect can be clearly seen for the symmetric wing chord, symmetric wing torsion, and antisymmetric wing bending roots.

It can be noted that the configuration "Twist−" increases the critical speed both for the SWC (> 37 knots) and AWB (> 39 knots) modes. The opposite trend is obtained with the "Twist+" configuration. Unfortunately, the improvement on whirl-flutter stability boundaries obtained with the configuration "Twist−" is penalized by the increment in the power required.

The twist distribution modifies the thrust per unit length over the blade, as shown in Fig. 11(a) for the flight condition at 300 knots. In particular, for the "Twist−" configuration the total thrust is shifted toward the blade tip increasing the

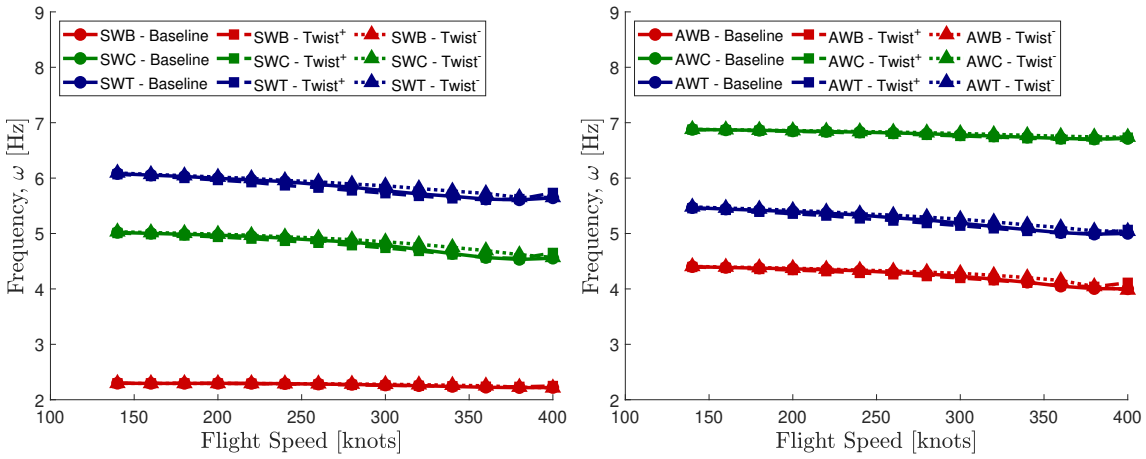

(a) Frequency – Symmetric roots.

(b) Frequency – Antisymmetric roots.

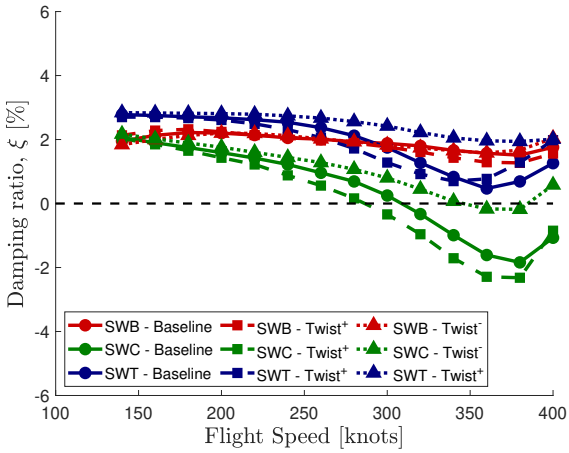

(c) Damping – Symmetric roots.

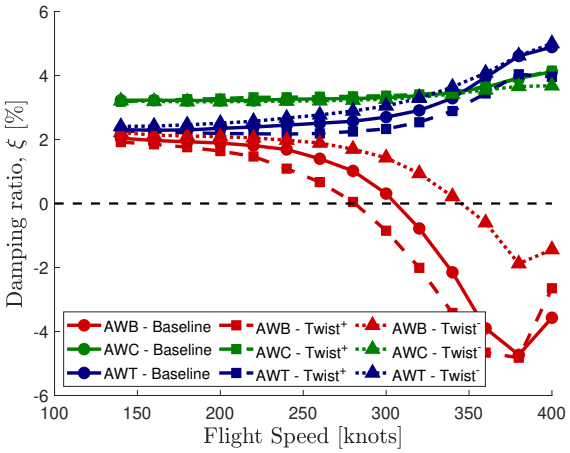

(d) Damping – Antisymmetric roots.

Fig. 10 Whirl-mode frequency and damping w.r.t. flight speed, level flight with unlimited power, 15% thin-wing.

total out-of-plane bending moment exerted at the blade root. As a consequence, the trim deformed coning angle due to blade elastic flapping, β_0^T, increases as well (Fig. 11(b)). A positive trim coning angle generates positive pitch-lag coupling $K_{P\zeta}$ (positive for lag back, pitch down), namely:

$$K_{P\zeta} = -\frac{\Delta\vartheta}{\Delta\zeta} = \frac{\left(\nu_\beta^2 - 1\right)\beta_0^T}{\hat{I}_p \nu_\vartheta^2}, \tag{2}$$

where ν_β is the natural frequency of the rotor coning mode (/rev), $\hat{I}_p$ is the dimensionless pitch moment of inertia and ν_ϑ is the pitch natural frequency (/rev). In turn, the positive $K_{P\zeta}$ improves whirl-flutter stability boundaries, as reported by Johnson in Ref. [40]. It must be remembered that the total collective flap angle is due to the precone angle $\beta_0^P = 1.5$ deg., plus the trim coning angle, i.e. $\beta_0 = \beta_0^P + \beta_0^T$. So, if the rotor has an ideal precone, then $\beta_0^T = 0$, and there would be no pitch/lag coupling. In APMODE, the proprotor operates at very low aerodynamic loading, while the precone is

designed for the high loading of hover. Hence, β_0^T is generally small or negative for the proprotor in cruise and there is a finite, negative pitch/lag coupling that limits the whirl-flutter speed.

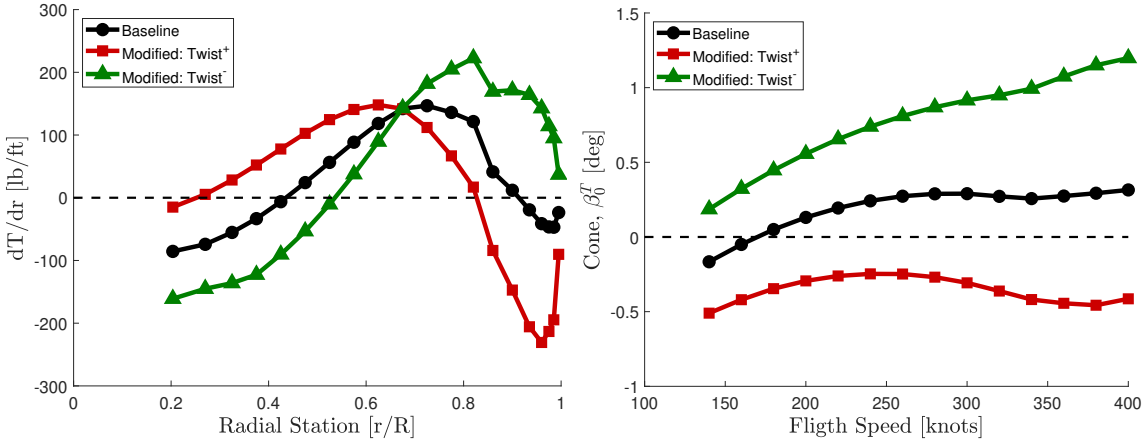

(a) Thrust distribution at 300 knots.

(b) Rotor coning.

Fig. 11 Rotor loads and coning angle - level flight with unlimited power, 15% thin-wing.

The "Twist−" configuration produces a reduction of the negative, or in some cases a positive, β_0^T angle improving the whirl-flutter stability. The opposite behavior is obtained with the "Twist+" configuration resulting in reduced stability boundaries. However, the non-ideal distribution of forces on the blade sections, due to the modified twist distribution, returns a higher local induced drag increasing the power required. Additional analyses performed in windmill trim conditions and reported in [14] confirmed that the "Twist−" shows a stabilizing effect, leading to similar increases in the whirl-flutter speed experienced by unlimited-power cases, both for symmetric and antisymmetric modes.

A preliminary run of optimizations for the level flight conditions with unlimited power was attempted in [14] using as optimization variables the twist slopes of up to three pre-assigned segments of the blade span. All optimizations led to significant extensions of the whirl-flutter speed (+17%), but with a remarkable penalization (+20%) in terms of the power required. For this reason, it was decided to tackle the problem by adding a new design variable into the optimization framework, considering the possibility to trade the advantages in terms of flight envelope extension obtained by a non-ideal twist distribution with the effects on the power required and torsional stiffness, so on whirl-flutter stability, that can be obtained by changing the wing airfoil thickness.

IV. Aircraft Optimization

Similar results to those presented in section III can be obtained by increasing the wing airfoil thickness, which also leads to an extension of the flutter-free envelope and an increase in power required. For this reason, it has been decided to extend the optimization presented in [14] considering, together with the blade twist distribution, the wing airfoil thickness as an additional design variable. To allow the correct exploration of the design space, the optimization has

been performed considering the extension of the whirl-flutter-free envelope as a cost function, including the constraint that the power required at the maximum safe flight speed must not exceed that of the baseline configuration, as indicated in Eq. (3). In this way, it is expected to leave to the optimizer to solve the dilemma between an increase in wing airfoil thickness or a change of blade twist slope.

A. Optimization Algorithm

The optimization process aims to maximize the whirl-flutter speed V_{wf}, under the constraint of keeping the power below a maximum value P_{ms}. Speed and power are expressed concerning the respective baseline values, i.e. V_{wf_0} and P_{ms_0}, to work with small and comparable values in the objective and constraint functions. The power value to limit is always the power required to fly at the maximum safe flight speed, i.e. at a speed 15% smaller than the whirl-flutter speed, $V_{ms} = V_{wf}/1.15$. In this way, it is possible to increase the maximum safe flight speed V_{ms} without using a more powerful powerplant. The resulting constrained minimization problem is:

$$\min_{\mathbf{x}} \frac{V_{wf_0}}{V_{wf}(\mathbf{x})}, \tag{3a}$$

$$\text{subject to } \frac{P_{ms}(\mathbf{x})}{P_{ms_0}} - 1 < 0, \quad \text{and} \quad lb_i < x_i < ub_i \qquad \forall i = 1, \ldots, n \tag{3b}$$

where $\mathbf{x} \in \mathbb{R}^n$ is the vector of optimization variables that may include the description of the blade twist slope, ϑ'_{tw_i}, represented through a piecewise linear law, the radial station where the slope change takes places, r_i, and the wing airfoil thickness t/c. The values lb_i and ub_i are the lower and upper bounds for each optimization variable.

Three different blade twist configurations have been proposed. In configuration #1 (Fig. 12(a)), a simple modification on the twist slope is proposed so that $\mathbf{x} = \left\{\vartheta'_{tw_1}, t/c\right\}$. Configurations #2 and #3 (see Fig. 12(b) and Fig. 12(c)) divide the blade respectively into two and three segments with different slopes on the twist laws. The number of optimization variables, including the wing airfoil thickness, increases up to six. Indeed, it must be pointed out that all blades are characterized by the same twist laws. More detailed blade twist laws have not been considered to avoid having a large number of design variables that could not have been managed by the optimization algorithm chosen.

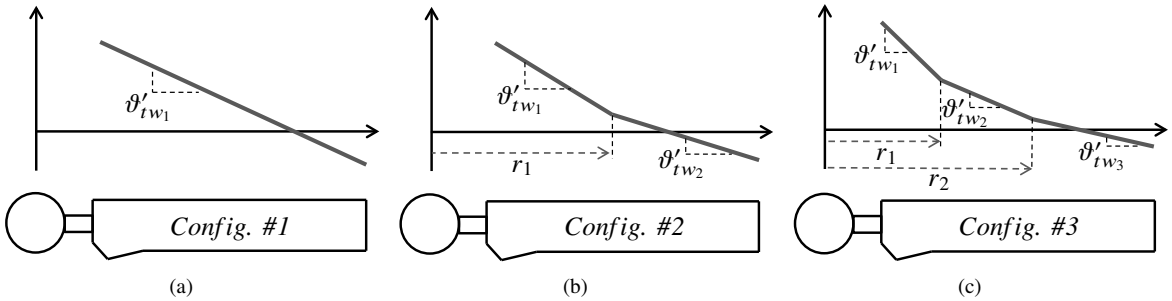

Fig. 12 Blade twist configurations.

The nonlinear constrained optimization of Eq. (3) is solved using the Interior Point Algorithm [41] implemented in Matlab, which showed good rates of convergence with a limited number of iterations. To evaluate the objective function it is necessary for each iteration to compute the whirl-flutter speed V_{wf}, the maximum safe flight speed V_{ms}, and the maximum power required P_{ms} using the current **x** vector. All gradients necessary to run the optimization algorithm have been computed using finite difference approximations. This has been possible with a limited computational cost thanks to the limited number of design variables considered. It is well known that the formulation proposed for the objective function through Eq. (3) may lead to a non-smooth function due to flutter mode switching between different design configurations, so further extension of this optimization problem to more accurate aircraft models or to cases with more design variables should consider specific gradient-based formulations, as those proposed in Refs. [42, 43].

So, the process starts with the evaluation of wing structural modes and natural frequencies through a NASTRAN analysis and the computation of aerodynamics coefficients using the expressions described in II.B.1 and II.B.2. Next, the CAMRAD/JA input file is built for a specific blade twist law and wing airfoil thickness t/c ratio. After the post-processing of the CAMRAD/JA results it is possible to evaluate the objective and constrain functions of Eq. (3) and compute a new optimization vector to restart the process until a minimum is reached. The block diagram in Fig. 13 summarizes the optimization process.

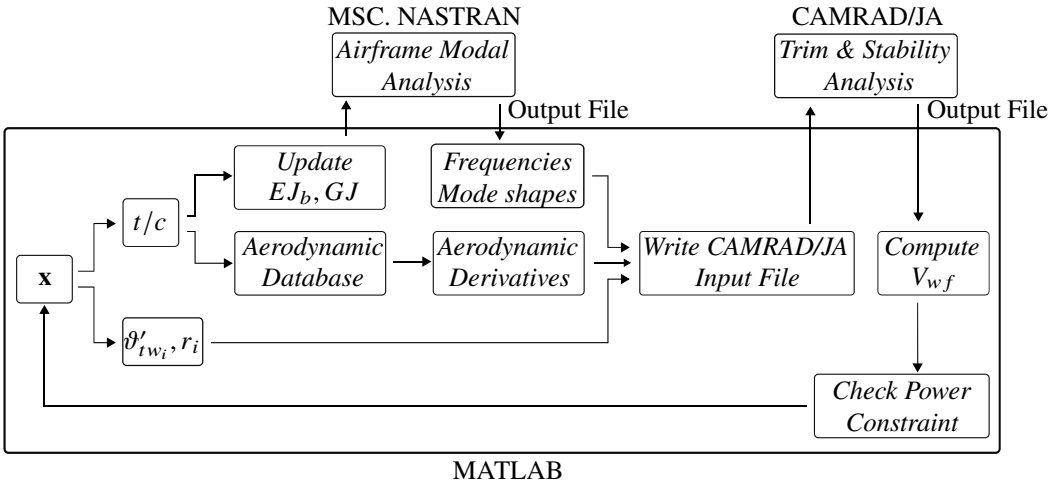

Fig. 13 Block diagram of the optimization procedure.

B. Optimization Results

The reference values are those obtained with the nominal ATB twist distribution and the 15% thin-wing, i.e. V_{wf_0} = 306 knots, V_{ms} = 266 knots, and P_{ms_0} = 891 hp.

The optimization showed that the objective function of Eq. (3) contains several local minima, so multiple attempts have been run starting from different randomly generated initial guesses (#6 for each configuration) to scan the full

design space. The optimized results obtained for the three-blade twist configurations are summarized in Table 7. It must be highlighted that all solutions were practically on the limit of the power required. They were not exactly at 100% due to convergence issues of the CAMRAD/JA trim algorithm at high speed. Multiple failures in finding a correct trim solution limited the capability of the Matlab optimization algorithm to compute gradients through finite differences, reducing the possibility to explore entirely the solution space. Improvements can be expected by the implementation of the same optimization procedure with other, more recent, aeromechanic solvers (see Ref. [44]).

Table 7 Aircraft optimization results summary.

Config.	$\frac{\vartheta'_{tw_1}}{\vartheta'_{tw_0}}$	$\frac{\vartheta'_{tw_2}}{\vartheta'_{tw_0}}$	$\frac{\vartheta'_{tw_3}}{\vartheta'_{tw_0}}$	$\frac{r_1}{R}$	$\frac{r_2}{R}$	t/c	V_{wf}	$\frac{V_{wf}}{V_{wf0}} - 1$	Mode	P_{ms}	$\frac{P_{ms}}{P_{ms0}}$
[#]	[n.d.]	[n.d.]	[n.d.]	[%]	[%]	[%]	[knots]	[%]		[hp]	[%]
OPT-1	1.03	–	–	–	–	17	359	17.6	SWC	886	99.5
OPT-2	1.25	0.70	–	52	–	17	365	19.4	SWT	875	98.3
OPT-3	1.17	1.07	0.93	40	48	17	370	21.0	SWC	873	98.0

When considering the simplest configuration with a linear twist, the optimization routine increases the wing airfoil thickness (17% t/c) to raise the whirl-flutter speed. As a consequence, the twist slope is slightly increased compared to the baseline twist distribution, i.e. $\vartheta'_{tw_1}/\vartheta'_{tw_0} = 1.03$, to reduce the increment of power due to the higher drag generated by the thicker wing. This solution leads to a significant extension of the flutter-free envelope (+17.6%). Besides, the power required is contained to the twist slope increment.

Giving more freedom to the blade twist law allows increasing the flutter-free envelope by another 6 to 11 knots while still keeping the power limited (see OPT-2 and OPT-3 in Tab. 7). Once again, the optimization routine increases the wing airfoil thickness to 17%. However, the optimized configurations with piecewise linear twist laws are now characterized by an increment of the twist slope on the inboard sections while the twist slope is reduced on the outboard sections. These modifications allow us to further increase the whirl-flutter speed through the mechanism discussed in the previous section. Unfortunately, the already reported limited robustness of the solver CAMRAD/JA in finding trim conditions beyond the limits of the flight envelope affected in particular the possibility to explore in depth the design space with the three-slope configuration.

The $V - \xi$ plots for the three optimized configurations are shown in Fig. 14. Symmetric and antisymmetric roots are compared with the eigenvalues of the baseline configuration with reference to the flight speed. All the optimized configurations show that the AWB root is more stable when compared to the baseline configuration thanks to the thicker wing, which provides a higher frequency separation between the wing beam bending and torsion modes, as highlighted by Nixon in Ref. [3]. The same effect, but less remarked, is presented for the SWB and SWC modes.

Among all the optimized configurations, the OPT-2 returns the highest flapwise bending moment at the blade root,

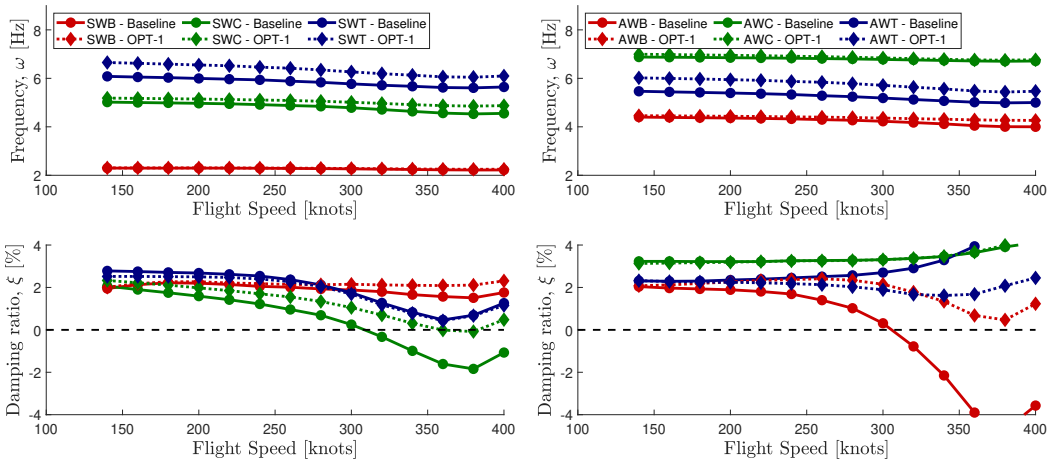

(a) OPT-1 – Symmetric roots.

(b) OPT-1 – Antisymmetric roots.

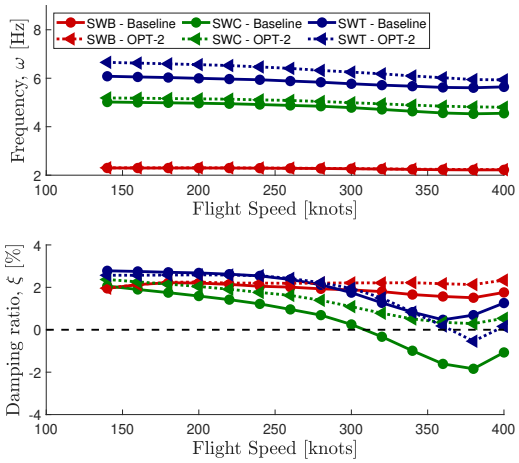

(c) OPT-2 – Symmetric roots.

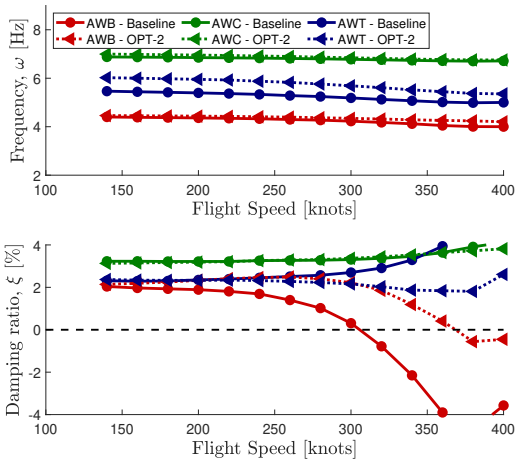

(d) OPT-2 – Antisymmetric roots.

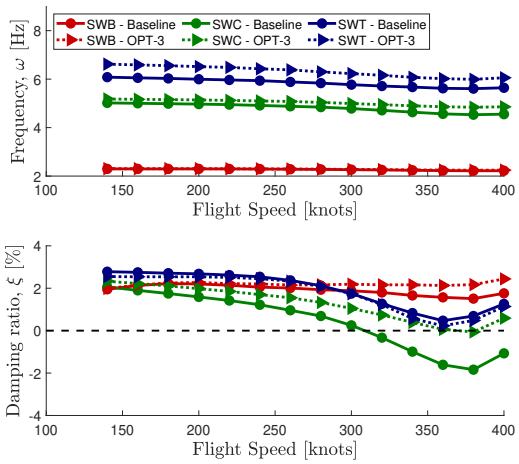

(e) OPT-3 – Symmetric roots.

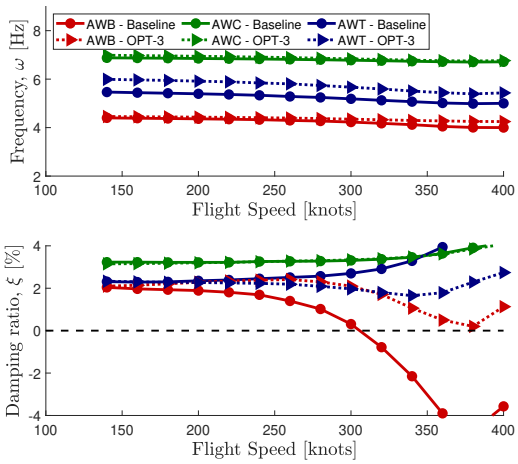

(f) OPT-3 – Antisymmetric roots.

Fig. 14 Whirl-mode frequency and damping w.r.t. flight speed for the optimized configurations.

hence the highest trim coning angle, increasing further the pitch-lag coupling (see Eq. 2) and modifying the SWT modal participations. The main symmetric modal participation factors of the aeroelastic SWT mode at 380 knots for the three optimized configurations are shown in Fig. 15, normalized by setting the airframe SWT = 1. It is found that the aeroelastic SWT mode, which drives the whirl flutter for the optimized configuration OPT-2, provides the highest participation of the symmetric lead-lag cyclic cosine mode (ζ_{1C}). Indeed, its contribution is 20% greater than the other optimized configurations and even more significant than the airframe SWT modal participation. The lead-lag cyclic motion shifts the center of gravity of the rotor from its center (as for the ground resonance in helicopters, see Ref. [39], Chapter 20), exciting the SWT mode. This mechanism reduces the damping of the aeroelastic SWT, providing a switch on the whirl-flutter onset between SWC and SWT for the optimized configuration OPT-2.

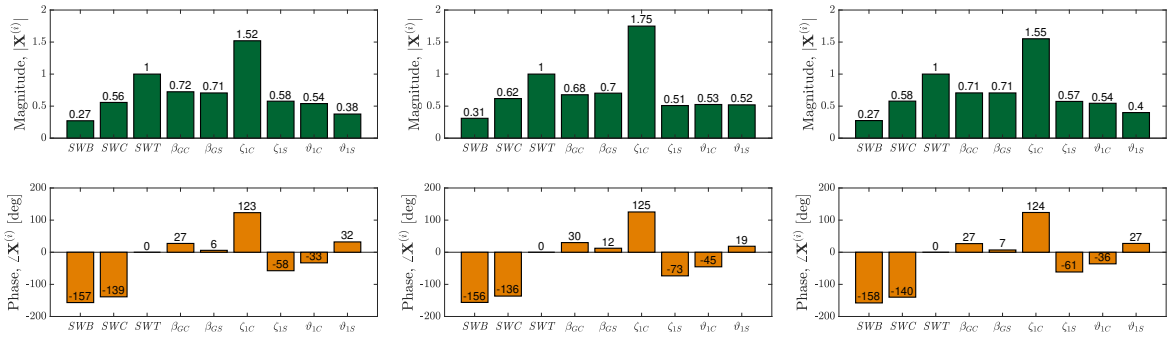

(a) OPT-1. (b) OPT-2. (c) OPT-3.

Fig. 15 Main symmetric modal participation factors of the aeroelastic SWT mode at 380 knots for the optimized configurations.

The blade sectional loads computed for the three optimized configurations and depicted in Fig. 16 can help the reader to figure out the impact of twist modifications on the power required and stability proneness. Section forces and bending moments are computed on the rotating shaft reference frame at 300 knots for the normal and inplane mean components. With this reference frame, the blade radial stations are measured along the y-axis, starting from the blade root up to the tip. Inplane loads are computed along the x-axis, positive along the blade trailing edge. Normal loads are evaluated along the z-axis, positive upward and orthogonal to the rotor shaft plane.

Both configurations OPT-2 and OPT-3 shift the rotor thrust toward the blade tip (Fig. 16(a)) when compared to the baseline configuration. Although the total thrust remains the same, as remarked by the vertical shear force evaluated at the blade root (see Fig. 16(b)), the corresponding flapwise bending moments are larger (Fig. 16(c)), increasing the blade trim coning angle and the pitch-lag coupling, as well as the whirl-flutter speed. The inplane sectional forces along the blade span are also modified by the twist distributions, as shown in Fig. 16(d). However, the optimized configurations return the same lagwise bending moments at the blade root (see Fig. 16(f)), avoiding any increment in the power required.

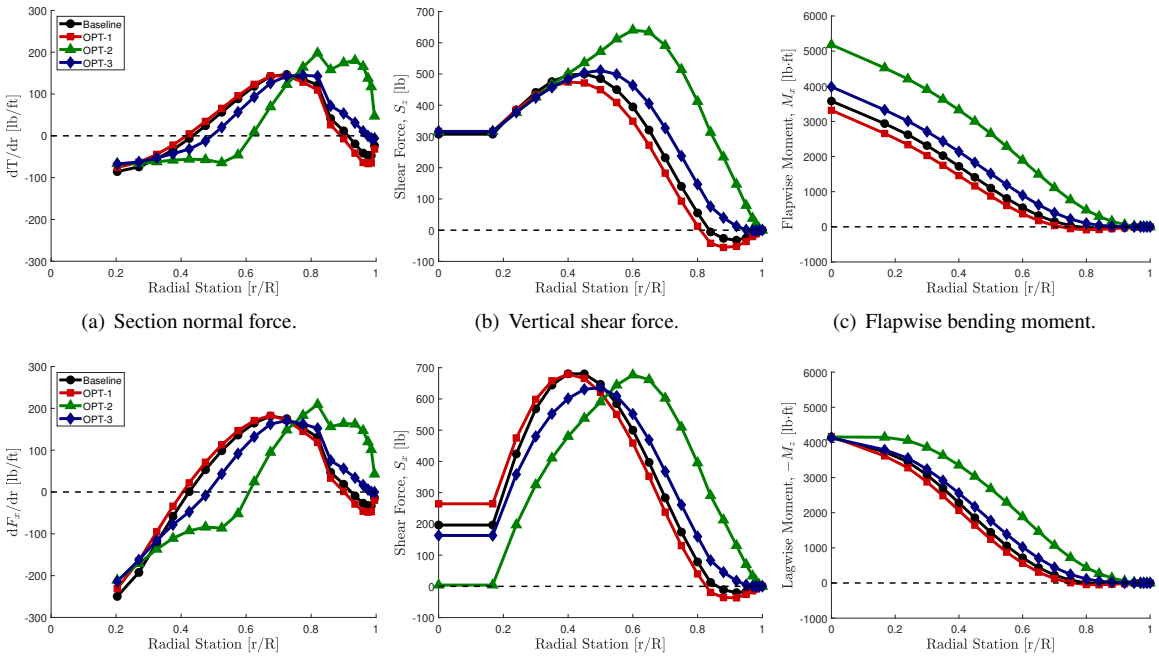

(a) Section normal force. (b) Vertical shear force. (c) Flapwise bending moment.

(d) Section inplane force. (e) Inplane shear force. (f) Lagwise bending moment.

Fig. 16 Normal (top) and inplane (bottom) rotor loads for the optimized configurations - 300 knots.

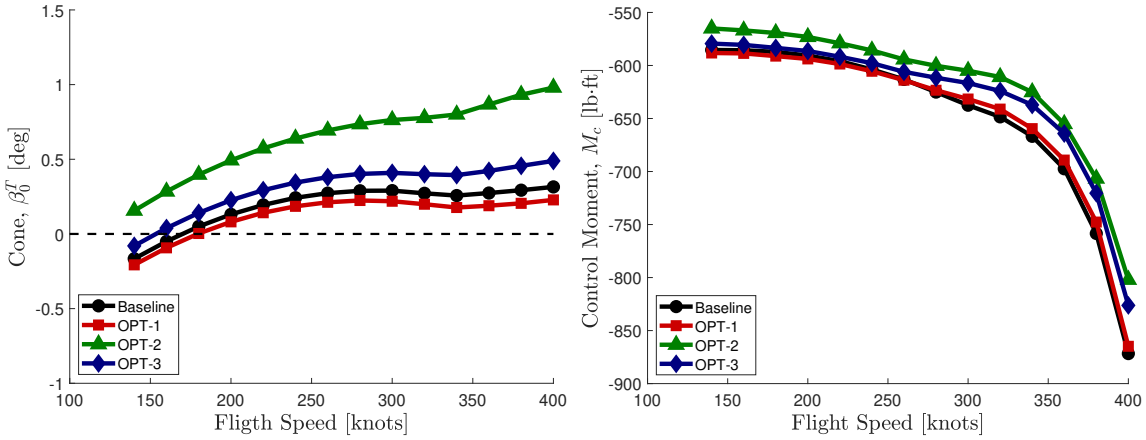

(a) Rotor coning. (b) Control moment.

Fig. 17 Rotor coning and control moments for the optimized configurations – level flight with unlimited power.

The rotor coning and the control moment measured at the blade cutout are shown in Fig. 17 with reference to the flight speed. The highest trim coning angles are obtained for the two segments' optimized solution (OPT-2), where the twist modification is more significant, as well as the rotor loads along the blade span. Finally, it must be remarked the change produced in the pitch control moment: it decreases for all flight speeds, reducing the load on the rotor pitch link, as shown in Fig. 17(b). This is in contrast with the effect generated by the usage of swept-tip blades reported in Refs. [12, 13] that lead always to an increase in pitch link loads. Indeed, acting on the blade twist distribution the

aerodynamic center is not shifted along the chord direction but simply rotated about the blade feathering axis.

C. Assessment of the Effects for Different Trim Conditions

While the analysis in level flight with unlimited power was helpful to understand the physics of the relationship that exists between the blade twist and the whirl flutter, the trim conditions considered are not fully representative of what happens with real flying aircraft.

Consequently, trim and stability analyses have been recomputed for limited power conditions, considering the baseline and the optimized configurations of Table 7, to verify the robustness of the proposed solutions. For the sake of completeness, windmilling conditions have been considered as well. Whirl-flutter speeds and the corresponding mode shapes are summarized in the bar charts of Fig. 18. Both limited power and windmilling conditions reduce the

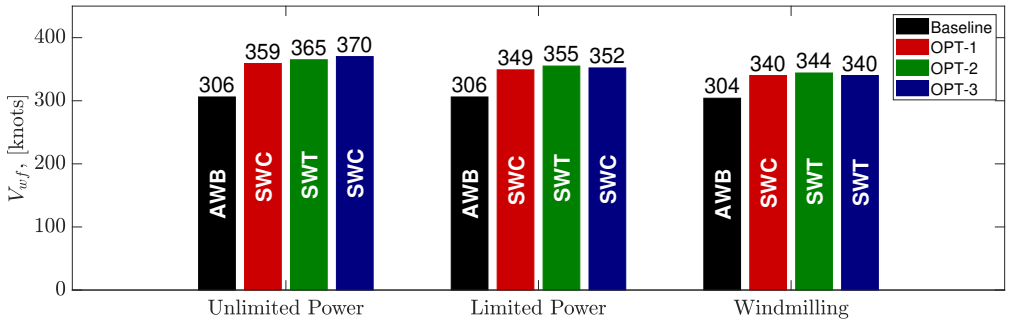

Fig. 18 Whirl-flutter speeds for the optimized configurations obtained at different trim conditions.

stability boundaries, although the optimized configurations are still able to increase the critical speeds when compared to the baseline configuration. As expected, the worst-case scenario is due to the windmilling conditions. Indeed, the increment on the whirl-flutter speed is reduced to 13%.

The trim parameters for the optimized configurations with limited power are depicted in Fig 19. The power limit is set to the maximum continuous power supplied by the Lycoming LTC1K-41K turboshaft engine, equal to 1550 hp. From the previous results, it can be observed that up to 320 knots the power required is less than the maximum continuous power (see Fig. 9(a)). At higher flight speeds, the aircraft starts to dive to reach the target speed set by the trim analysis. The trim conditions show the negative climb angle above 320 knots (Fig. 19(a)) and the consequent reduction of thrust (Fig. 19(b)). This, in turn, is the root cause of the fast decrease of the rotor coning angle, as shown in Fig. 19(c), which is probably the main responsible for the reduction of the whirl-flutter speed.

Free-flight windmilling conditions are allowed only in a descending flight. Indeed, the climb angles shown in Fig. 20(a) are negative at any flight speed. The zero-power condition provides negative thrust values (see Fig. 20(b)) and the corresponding rotor coning angles are reduced when compared to powered trim conditions. Nonetheless, the optimized configurations with multiple twist slopes are still able to provide higher trim coning angles compared to the baseline configuration, as depicted in Fig. 20(c). It must be remarked that all the optimized configurations are also

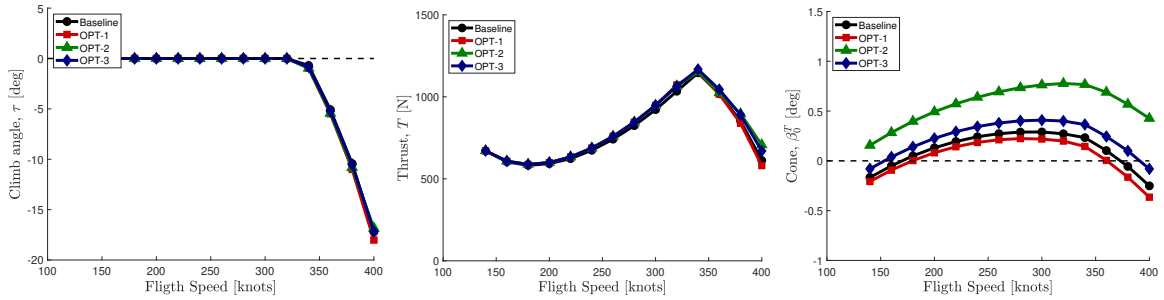

(a) Climb angle. (b) Thrust. (c) Rotor coning.

Fig. 19 Trim parameters for the baseline and optimized configurations – Limited power.

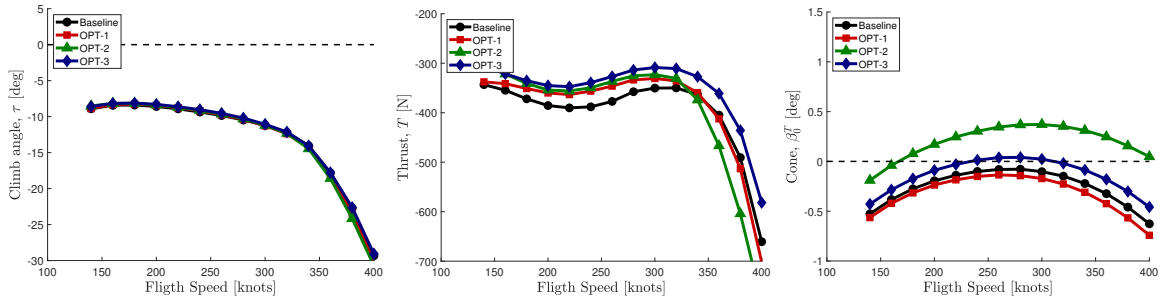

(a) Climb angle. (b) Thrust. (c) Rotor coning.

Fig. 20 Trim parameters for the baseline and optimized configurations – Windmilling.

characterized by a thicker wing, which is also responsible for the whirl-flutter speed increment.

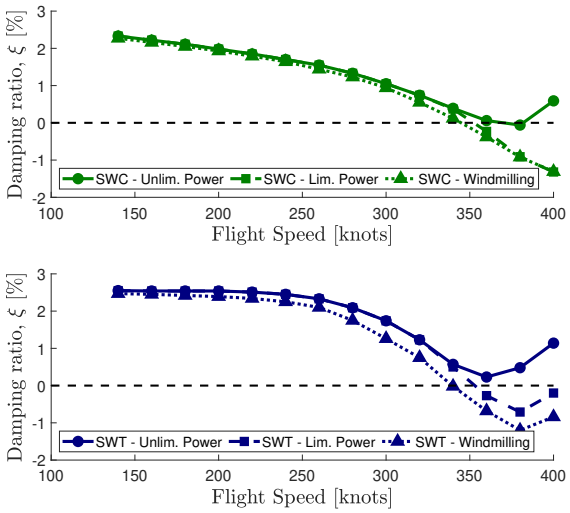

Fig. 21 SWC and SWT damping w.r.t. flight speed obtained for the optimized configuration OPT-3 at different trim conditions.

Finally, it should be noted that the whirl-flutter mode switches for the optimized configuration OPT-3 when moving from powered to unpowered cases. Indeed, the most critical whirl-flutter onset for the OPT-3 powered conditions is the

SWC mode, although the SWT also shows a destabilizing trend at high flight speed, as depicted in Fig. 14(e). The windmilling condition reduces the damping of the two symmetric roots compared to powered conditions (see Fig. 21). However, the damping ratio of the SWT in windmilling conditions starts to deviate from the powered curves before the SWC, anticipating the intersection with the zero damping axis of about 5 knots. A similar effect is obtained for the optimized configuration with a single twist slope (OPT-1), although the corresponding SWT mode in powered conditions is more stable than the SWC with the result that the damping reduction due to the zero power condition does not cause any mode switching.

D. Assessment of the Effects in Helicopter Mode

The previous section showed how a modification in the twist angle distribution along the blade and on the wing airfoil thickness can positively influence the whirl-flutter boundaries, without penalties on the power required. However, to understand if the proposed design changes are affordable it is necessary to assess also the effects in HEMODE. For tiltrotors, this condition is crucial since it allows vertical take-off/landing and the possibility to hover.

CAMRAD/JA settings are consequently modified to perform the trim analysis in HEMODE mode for the baseline (15% thin-wing) and the optimized configurations. It has been decided to run a trim analysis between 0 and 80 knots, the maximum speed for the HEMODE configuration (see Ref. [4]), to verify that no significant penalizations in terms of the power required are obtained using the modified configurations. Trim results are shown in Fig. 22. Figure 22(b) shows how the power required in the HEMODE flight conditions is lower for the solutions that have a reduced slope in the blade tip, namely for the optimized configurations OPT-2 and OPT-3. For these two cases, the modification of the blade twist leads to a slight increment of induced power, although the profile power is reduced so that the overall power required decreases. A benign effect is also observed on the rotor coning angles (Fig. 22(c)) and on the control moments (Fig. 22(d)).

V. Conclusions

A detailed XV-15 aeroelastic tiltrotor model, with Advanced Technology Blades, has been analyzed with CAMRAD/JA to examine the effects on whirl-flutter stability boundaries and power required of different blade twist configurations and different wing airfoil thickness values. The XV-15 airframe has been modified to have a reference model with a thinner wing (15% t/c) to better reveal the effects on whirl-flutter boundaries. To identify the best design, an optimization algorithm has been set up to explore the design space, considering the wing airfoil thickness and the blade twist as design variables with the objective of maximizing the whirl-flutter speed of the aircraft without requiring an increment of the power required. The first element highlighted by the optimization has been the tendency to increase the wing airfoil thickness to values close to 17% to increase the overall stability of whirl-modes without increasing significantly the power required. The additional inclusion of a carefully defined blade twist has been able to further

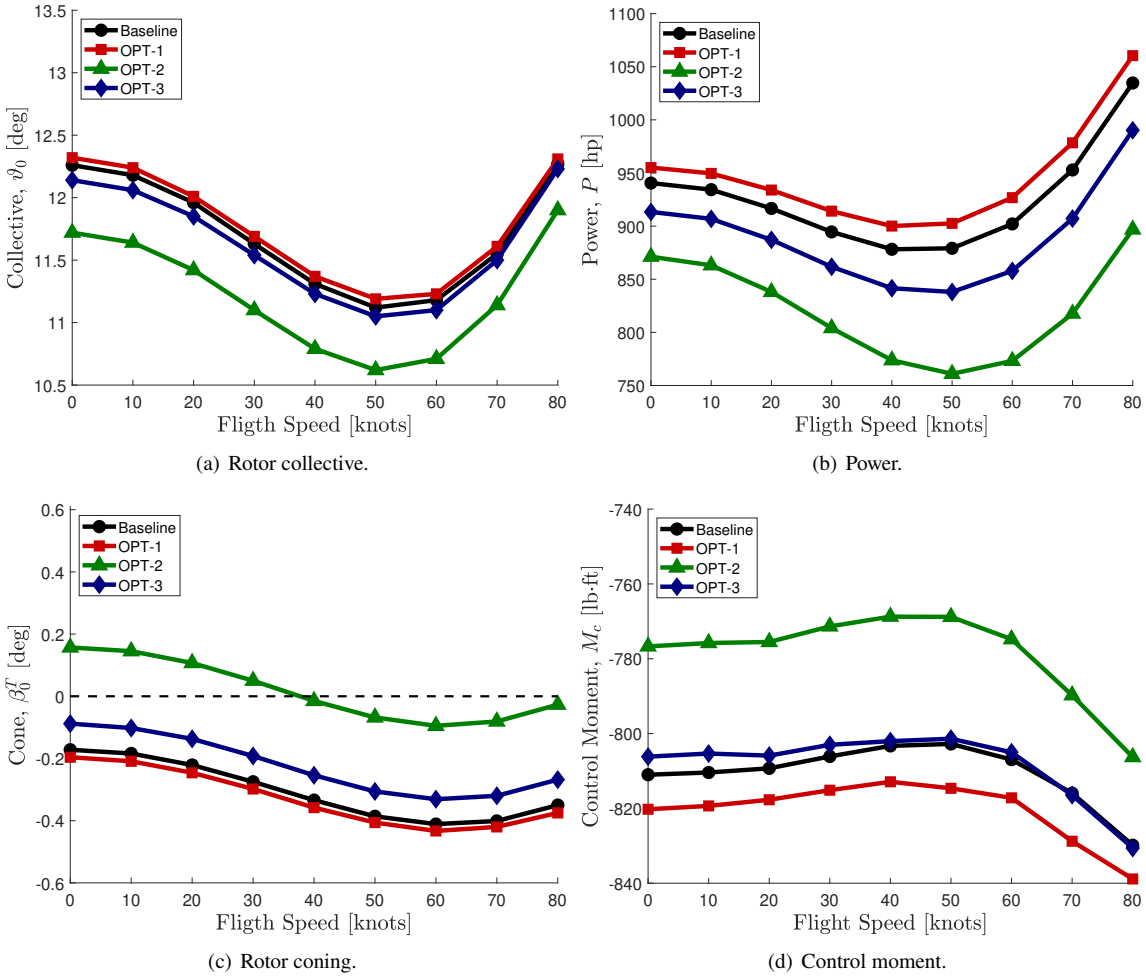

(a) Rotor collective.

(b) Power.

(c) Rotor coning.

(d) Control moment.

Fig. 22 Trim conditions in helicopter mode.

increase the flutter-free boundaries, without increasing the power required, through a twist slope decrease near the blade tip and a slope increase at the blade root. In fact, the modification of the distribution of thrust over the blade span, shifting the total blade thrust vector toward the blade tip, led to the increase of the flapwise bending moment at the blade root, and the consequent increase of the trim coning angle that has been identified as the responsible for the increased whirl-flutter stability. The rotor loads obtained with the optimized solutions with multiple twist slopes increased the flapwise bending moments generated in forward flight at values that are still well below those experienced by the blades in helicopter mode. The lagwise bending moment is kept constant at the blade root, avoiding any increment of power required. Conversely, the impact of the optimal twist on rotor pitch link loads has been assessed as benign, since the section aerodynamic center is not shifted along the chord direction, but rotated about the blade feathering axis. This effect makes these solutions more attractive than the use of a sweep angle added at the blade tip. Finally, it has been verified that the proposed design changes do not impact negatively the helicopter mode performance, particularly on the power required.

In conclusion, it is possible to affirm that all analyses performed showed a clear influence of the blade twist angle on the whirl-flutter stability. Given the positive impact that this parameter may have on the aircraft performance and specifically in terms of the power required, the blade twist angle should be considered as one of the basic design parameters to be kept into account at the level of conceptual assessment of a tiltrotor configuration, together with other more classical parameters like wing airfoil thickness and torsional stiffness. The preliminary optimization presented here showed how it is possible to identify some sweet spots, where a careful selection of the blade twist leads to improvements in terms of extension of the flutter-free flight envelope, as well as reductions of the power required. Further optimizations, based on a more accurate optimization algorithm and simulation model may identify optimal configurations that can fit the operational objectives of the aircraft to be designed.

More generally, an increase in whirl-flutter stability, even if linked to a limited increase of the power required, could be traded with the advantages obtained by the possibility to extend the flight envelope of a tiltrotor. Consequently, further and more accurate investigations of the design options on specific aircraft configurations are required, to fully assess the potential of this additional design variable.

References

[1] Taylor, E., and Browne, K., "Vibration Isolation of Aircraft Power Plants," *Journal of the Aeronautical Sciences*, Vol. 6, No. 2, 1938, pp. 43–49. https://doi.org/10.2514/8.760.

[2] Reed III, W., "Propeller-Rotor Whirl Flutter: A State-of-the-Art Review," *Journal of Sound and Vibration*, Vol. 4, No. 3, 1966, pp. 526–530. https://doi.org/10.1016/0022-460X(66)90142-8.

[3] Nixon, M. W., "Parametric Studies for Tiltrotor Aeroelastic Stability in Highspeed Flight," *Journal of the American Helicopter Society*, Vol. 38, No. 4, 1993, pp. 71–79. https://doi.org/10.4050/JAHS.38.71.

[4] Maisel, M., "NASA/Army XV-15 Tilt-Rotor Research Aircraft Familiarization Document," Technical Memorandum X-62, 407, NASA Ames Research Center, Mountain View, CA, January 1975.

[5] Popelka, D., Lindsay, D., Parham, T., Berry, V., and Baker, D. J., "Results of an Aeroelastic Tailoring Study for a Composite Tiltrotor Wing," *Journal of the American Helicopter Society*, Vol. 42, No. 2, 1997, pp. 126–136. https://doi.org/10.4050/JAHS.42.126.

[6] Barkai, S., and Rand, O., "The Influence of Composite Induced Couplings on Tiltrotor Whirl Flutter Stability," *Journal of the American Helicopter Society*, Vol. 43, No. 2, 1998, pp. 133–144. https://doi.org/10.4050/JAHS.43.133.

[7] Nixon, M. W., Piatak, D. J., Corso, L. M., and Popelka, D. A., "Aeroelastic Tailoring for Stability Augmentation and Performance Enhancements of Tiltrotor Aircraft," *Journal of the American Helicopter Society*, Vol. 45, No. 4, 2000, pp. 270–279. https://doi.org/10.4050/JAHS.45.270.

[8] Van Aken, J. M., "Alleviation of Whirl-Flutter on Tilt-Rotor Aircraft Using Active Controls," *Proceedings of the 47th American Helicopter Society Annual Forum*, American Helicopter Society International, Fairfax, VA, 1991, pp. 1321–1344.

[9] Hathaway, E., and Gandhi, F., "Tiltrotor Whirl Flutter Alleviation Using Actively Controlled Wing Flaperons," *AIAA Journal*, Vol. 44, No. 11, 2006, pp. 2524–2534. https://doi.org/10.2514/1.18428.

[10] Paik, J., Singh, R., Gandhi, F., and Hathaway, E., "Active Tiltrotor Whirl-Flutter Stability Augmentation Using Wing-Flaperon and Swash-Plate Actuation," *Journal of Aircraft*, Vol. 44, No. 5, 2007, pp. 1439–1446. https://doi.org/10.2514/1.20234.

[11] Kambampati, S., and Smith, E., "Aeroelastic Optimization of High-Speed Tiltrotor Wings with Wing Extensions and Winglets," *Journal of Aircraft*, Vol. 54, No. 5, 2017, pp. 1718–1727. https://doi.org/10.2514/1.C034195.

[12] Acree Jr., C., Peyran, R., and Johnson, W., "Rotor Design Options for Improving Tiltrotor Whirl-Flutter Stability Margins," *Journal of the American Helicopter Society*, Vol. 46, No. 2, 2001, pp. 87–95. https://doi.org/10.4050/JAHS.46.87.

[13] Gul, S., and Datta, A., "Aeroelastic Loads and Stability of Swept-Tip Hingeless Tiltrotors toward High-Speed Instability-Free Cruise," *Journal of the American Helicopter Society*, Vol. 68, No. 1, 2023, pp. 1–18. https://doi.org/10.4050/JAHS.68.012001.

[14] Muscarello, V., and Quaranta, G., "Optimization of Tiltrotor Blade Twist to Increase Whirl-Flutter Stability," *AIAA Science and Technology Forum*, American Institute of Aeronautics and Astronautics, Inc., Reston, VA, 2019, pp. 1–15. https://doi.org/10.2514/6.2019-1366.

[15] McCarthy, T., and Chattopadhyay, A., "A Coupled Rotor/Wing Optimization Procedure for High Speed Tilt-Rotor Aircraft," *Journal of the American Helicopter Society*, Vol. 41, No. 4, 1996, pp. 360–369. https://doi.org/10.4050/JAHS.41.360.

[16] Stettner, M., and Schrage, D., "An Approach to Tiltrotor Wing Aeroservoelastic Optimization Through Increased Productivity," *Proceedings of the 4th Symposium on Multidisciplinary Analysis and Optimization*, American Institute of Aeronautics and Astronautics, Inc., Reston, VA, 1992, pp. 749–759. https://doi.org/10.2514/6.1992-4781.

[17] Orr, S., and Hajela, P., "Genetic Algorithm-Based Collaborative Optimization of a Tiltrotor Configuration," *Proceedings of the 46th AIAA/ASME/ASCE/AHS/ASC Structures, Structural Dynamics and Materials Conference*, American Institute of Aeronautics and Astronautics, Inc., Reston, VA, 2005, pp. 5982–5993. https://doi.org/10.2514/6.2005-2285.

[18] Kambampati, S., Hoover, T., Smith, E. C., and Maughmer, M. D., "Multidisciplinary Optimization for High-Speed, High-Efficiency Tiltrotors with Wing Extensions," *American Helicopter Society Specialists' Conference on Aeromechanics Design for Vertical Lift 2016*, American Helicopter Society International, Fairfax, VA, 2016, pp. 475–484.

[19] Park, J., Kim, S., Jung, S., and Lee, M., "Design and Analysis of Variable-Twist Tiltrotor Blades Using Shape Memory Alloy Hybrid Composites," *Smart Materials and Structures*, Vol. 20, No. 1, 2011. https://doi.org/10.1088/0964-1726/20/1/015001.

[20] Acree, C. W., "An Improved CAMRAD Model for Aeroelastic Stability Analysis of the XV-15 with Advanced Technology Blades," Technical Memorandum 4448, NASA Ames Research Center, Mountain View, CA, March 1993.

[21] Maisel, M. D., Giulianetti, D. J., and Dugan, D. C., *The History of the XV-15 Tilt Rotor Research Aircraft: From Concept to Flight*, The NASA History Series, Washington, D.C., 2000, Chap. Flight Research, pp. 65–82.

[22] Johnson, W., *CAMRAD/JA, A Comprehensive Analytical Model of Rotorcraft Aerodynamics and Dynamics, Johnson Aeronautics Version*, Johnson Aeronautics, Palo Alto, CA, 1988.

[23] Muscarello, V., and Quaranta, G., "Structural Coupling and Whirl-Flutter Stability with Pilot-in-the-Loop," *Journal of the American Helicopter Society*, Vol. 66, No. 3, 2021, pp. 1–16. https://doi.org/10.4050/JAHS.66.032003.

[24] Ferguson, S. W., "A Mathematical Model for Real-Time Flight Simulation of a Generic Tilt-Rotor Aircraft," Contractor Report 166536, NASA Ames Research Center, Mountain View, CA, September 1988.

[25] Masarati, P., Muscarello, V., and Quaranta, G., "Linearized Aeroservoelastic Analysis of Rotary-Wing Aircraft," *Proceedings of the 36th European Rotorcraft Forum*, Assoc. Aéronautique et Astronautique de France, Paris, France, 2010, pp. 1–10.

[26] Parham, T., Jr., and Corso, L. M., "Aeroelastic and Aeroservoelastic Stability of the BA 609," *Proceedings of the 25th European Rotorcraft Forum*, Associazione Italiana di Aeronautica e Astronautica, Rome, Italy, 1999, pp. 1–10. Paper G3.

[27] Gaffey, T. M., "The Effect of Positive Pitch-Flap Coupling (Negative δ_3) on Rotor Blade Motion Stability and Flapping," *Journal of the American Helicopter Society*, Vol. 14, No. 2, 1969, pp. 49–67. https://doi.org/10.4050/JAHS.14.2.49.

[28] Bilger, J., Marr, R., and Zahedi, A., "Results of Structural Dynamic Testing of the XV-15 Tilt Rotor Research Aircraft," *Journal of the American Helicopter Society*, Vol. 27, No. 2, 1982, pp. 58–65. https://doi.org/10.4050/JAHS.27.58.

[29] Pitt, D. M., and Peters, D. A., "Theoretical Prediction of Dynamic-Inflow Derivatives," *Vertica*, Vol. 5, No. 1, 1981, pp. 21–34.

[30] Schaeffer, J., Alwang, R., and Joglekar, M., "V-22 Thrust Power Management Control Law Development," *Proceedings of the 47th American Helicopter Society Annual Forum*, American Helicopter Society International, Fairfax, VA, 1991, pp. 1093–1100.

[31] Muscarello, V., and Quaranta, G., "Wing-Pilot Vertical Bounce in Tiltrotors," *Journal of Guidance, Control, and Dynamics*, Vol. 41, No. 8, 2018, pp. 1731–1743. https://doi.org/10.2514/1.G002960.

[32] Muscarello, V., Colombo, F., Quaranta, G., and Masarati, P., "Aeroelastic Rotorcraft–Pilot Couplings in Tiltrotor Aircraft," *Journal of Guidance, Control, and Dynamics*, Vol. 42, No. 3, 2019, pp. 1–14. https://doi.org/10.2514/1.G003922.

[33] Megson, T., *Aircraft Structures for Engineering Students*, fifth edition ed., Butterworth–Heinemann, UK, 2013, Chap. Structural Idealization, pp. 558–580.

[34] Bonetti, A., "Whirl Futter Stability Enhancement by Rotor Twist Optimization," Master's thesis, Politecnico di Milano, April 2020.

[35] Han, S. M., Benaroya, H., and Wei, T., "Dynamics of Transversely Vibrating Beams using four Engineering Theories," *Journal of Sound and Vibration*, Vol. 225, No. 5, 1999, pp. 935–988. https://doi.org/10.1006/jsvi.1999.2257.

[36] Katz, J., and Plotkin, A., *Low-Speed Aerodynamics*, Cambridge University Press, 2001, Vol. 13, Chaps. Three-Dimensional Small-Disturbance Solutions, pp. 167–205.

[37] Drela, M., "XFOIL: An Analysis and Design System for Low Reynolds Number Airfoils," *Low Reynolds Number Aerodynamics*, Springer, 1989, pp. 1–12.

[38] Liepmann, H. W., and Roshko, A., *Elements of Gasdynamics*, Dover Publication, Inc., Mineola, NY, USA, 2001.

[39] Johnson, W., *Rotorcraft Aeromechanics*, Cambridge University Press, New York, NY, USA, 2013, Chap. Hover, pp. 39–91.

[40] Johnson, W., "Analytical Modeling Requirements for Tilting Proprotor Aircraft Dynamics," Technical Note 8013, NASA Ames Research Center, July 1975.

[41] Waltz, R. A., Morales, J. L., Nocedal, J., and Orban, D., "An Interior Algorithm for Nonlinear Optimization that Combines Line Search and Trust Region Steps," *Mathematical programming*, Vol. 107, No. 3, 2006, pp. 391–408. https://doi.org/10.1007/s10107-004-0560-5.

[42] Jonsson, E., Riso, C., Lupp, C. A., Cesnik, C. E., Martins, J. R., and Epureanu, B. I., "Flutter and Post-Flutter Constraints in Aircraft Design Optimization," *Progress in Aerospace Sciences*, Vol. 109, 2019, p. 100537. https://doi.org/10.1016/j.paerosci.2019.04.001.

[43] Jonsson, E., Riso, C., Monteiro, B. B., Gray, A. C., Martins, J. R., and Cesnik, C. E., "High-Fidelity Gradient-Based Wing Structural Optimization Including Geometrically Nonlinear Flutter Constraint," *AIAA Journal*, 2023. https://doi.org/10.2514/1.J061575, In press.

[44] Johnson, W., "A History of Rotorcraft Comprehensive Analyses," *Proceedings of the 69th American Helicopter Society Annual Forum*, American Helicopter Society International, Fairfax, VA, 2013, pp. 685–706.